PHILOSOPHICAL TRANSACTIONS OF THE ROYAL SOCIETY A MATHEMATICAL, PHYSICAL & ENGINEERING SCIENCES

Geomagnetic Secular Variation and Fluid Motion at the Core Surface [and Discussion]

Kathryn A. Whaler and F. J. Lowes

Phil. Trans. R. Soc. Lond. A 1982 **306**, 235-246
doi: 10.1098/rsta.1982.0083

Phil. Trans. R. Soc. Lond. A **306**, 235–246 (1982) [235]
Printed in Great Britain

Geomagnetic secular variation and fluid motion at the core surface

By Kathryn A. Whaler
Bullard Laboratories, Department of Earth Sciences, Madingley Rise, Madingley Road, Cambridge CB3 0EZ, U.K.

The radial component of geomagnetic secular variation at the core surface is examined. Discrepancies between models for the same epoch are attributed in part to short-wavelength instabilities, and methods for producing smooth models are illustrated. Good core secular variation models are essential for inferring features of the core fluid flow, and two aspects are investigated here. Initially, a toroidal, azimuthal core–mantle boundary velocity field is assumed, which is tested for compatability with the geomagnetic data. Such a flow could be uniquely determined from the magnetic field and its secular variation. Purely toroidal motion implies no fluid upwelling at the core surface, and the data are consistent with this. The predominantly westward drift of the geomagnetic field prompted the assumption of azimuthal flow. However, this is not justified, as the magnitudes of the azimuthal and meridional velocity components are comparable at the few points for which this information is available.

1. Introduction

There have been several attempts to infer quantitative estimates of core motions from geomagnetic data (see, for example, Vestine 1952; Roberts & Scott 1965; Backus 1968; Booker 1969; Benton & Muth 1979; Benton 1979*a*, *b*, 1981). These investigations have been fraught with difficulties, for two main reasons. Firstly, extrapolation of the geomagnetic field from the Earth's surface to the core–mantle boundary (c.m.b.) is an unstable process. Secondly, even if the magnetic field and its secular change at the c.m.b. were perfectly resolved, the velocity field could not be deduced uniquely (Roberts & Scott 1965; Backus 1968). Both of these problems will be examined here, under the usual simplifying assumptions that the geomagnetic field is entirely of internal origin, and that the mantle is electrically insulating. Then the geomagnetic field, $\boldsymbol{B}$, outside the core can be expressed as the gradient of a potential, V, that satisfies Laplace's equation and whose solution can be expressed as a series of spherical harmonics. Field models derived from surface, or near-surface, data usually consist of a number of spherical harmonic coefficients, from which values of the field components can be synthesized at any point where the potential expansion is valid (see, for example, Barraclough & Malin 1971). For example, the radially outward component, B_r, which will be of particular interest here, can be written

$$B_r(r, \theta, \phi) = \sum_{l=1}^{L} (a/r)^{l+2} (l+1) \sum_{m=0}^{l} (g_l^m \cos m\phi + h_l^m \sin m\phi) P_l^m (\cos \theta), \qquad (1)$$

where (r, θ, ϕ) are spherical polar coordinates, a is the Earth's radius, P_l^m are associated Legendre functions, or spherical harmonics, and g_l^m, h_l^m are spherical harmonic coefficients, up to degree and order L. The same expression applies for $\dot{B}_r$, the time rate of change of the vertical component, with an appropriate set of spherical harmonic coefficients $\dot{g}_l^m$ and $\dot{h}_l^m$.

Using a spherical harmonic expansion as a basis, Whaler & Gubbins (1981) have developed techniques for smoothing the downward continuation process. In §2, the results of smoothing

the secular variation at the c.m.b. are compared with straightforward evaluation of (1), and with a method of Shure *et al.* (1982) for evaluating potential fields on surfaces within the Earth (by using an expansion in functions other than spherical harmonics). An attempt is made to distinguish between well resolved features and instabilities introduced by the data analysis and downward continuation procedures. The secular variation models are used in §§3 and 4 to investigate fluid motions at the top of the core with a view to reducing the inherent velocity ambiguity. One stage of this is achieved in §3, where it is shown that the models are consistent with no fluid upwelling at the core surface. In §4 I test the hypothesis that meridonal flow can be neglected; this, combined with the result of §3, would be sufficient to determine a unique

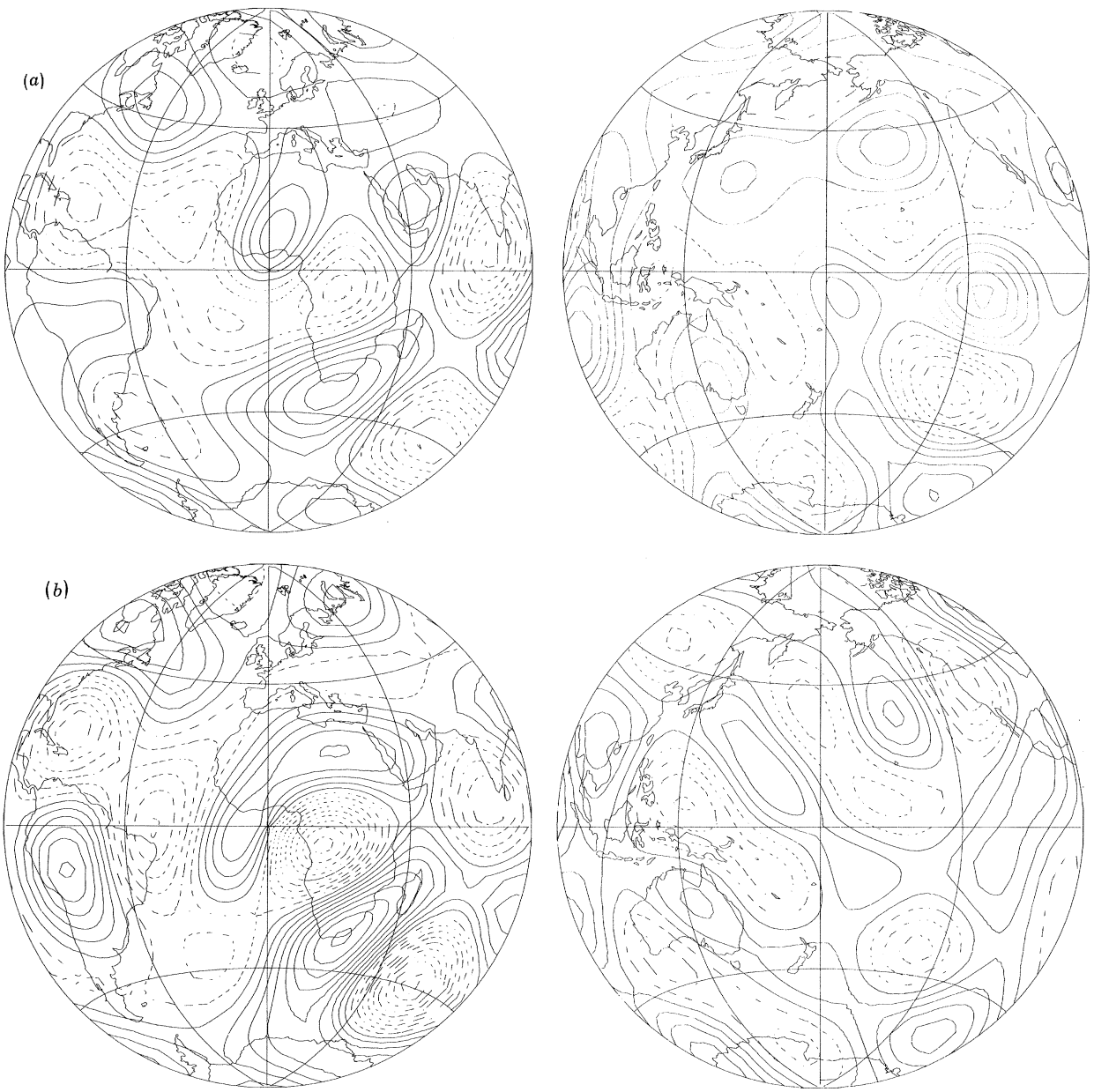

FIGURE 1(*a*) AND (*b*). For description see opposite.

PHILOSOPHICAL TRANSACTIONS OF THE ROYAL SOCIETY A MATHEMATICAL, PHYSICAL & ENGINEERING SCIENCES

velocity field. However, it is found that a purely azimuthal velocity field at the c.m.b. is not justified. An interesting consequence of this result is that the westward drift of the geomagnetic field is not associated with predominantly westward fluid flow. Gubbins (this symposium) discusses the implications of a westward-drifting geomagnetic field on core motions, and proposes a different hypothesis that, in principle, eliminates the velocity ambiguity.

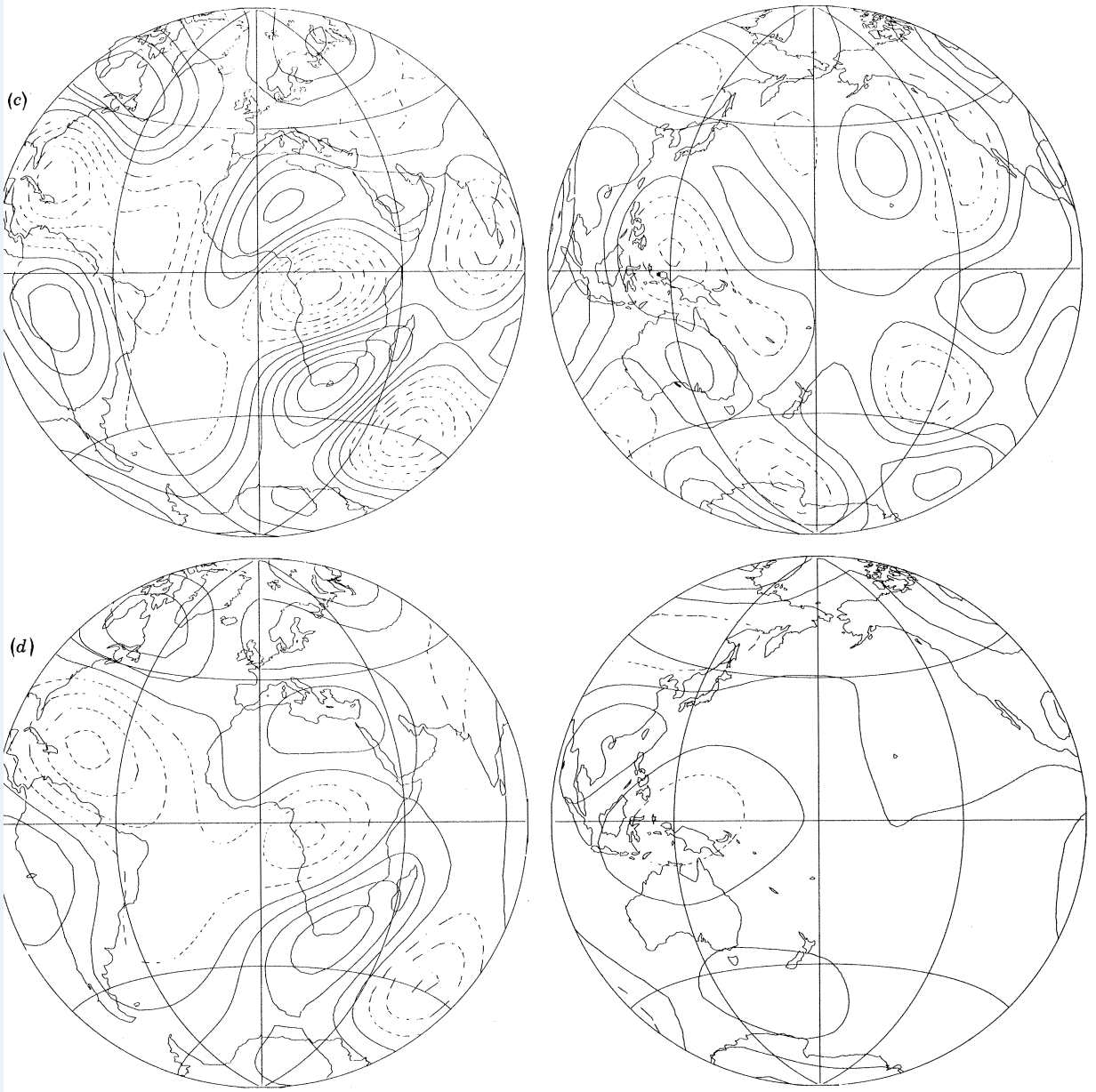

FIGURE 1. Radial component of secular variation at the c.m.b. The contour interval is 10^3 nT/year. Positive and zero contours are solid, negative contours dotted. (*a*) I.G.R.F.; (*b*) 'definitive' model; (*c*) 'definitive' model, smoothed; (*d*) small data set model using the Shure *et al.* (1982) method.

PHILOSOPHICAL TRANSACTIONS OF THE ROYAL SOCIETY A MATHEMATICAL, PHYSICAL & ENGINEERING SCIENCES

2. Secular variation at the core surface

An expression for the radial component of the magnetic field at the core surface is obtained by setting $r = r_c$, the radius of the core, in (1). This has the effect of multiplying the coefficients of the spherical harmonic expansion by $(a/r)^{l+2} \approx 2^{l+2}$, preferentially amplifying the higher order (shorter wavelength) harmonics. Unfortunately, the shorter wavelength coefficients are the least uncertain from an analysis of surface (and near-surface) magnetic data, and downward continuation can produce estimates of the fields dominated by short-wavelength instabilities from the extrapolation and amplification of errors in the higher harmonics. This is rarely a problem when analysing main field data because the quantity and quality usually ensure sufficiently good estimates of the higher degree and order coefficients. For the secular variation, however, the situation is rather different. Considerable weight must be attached to permanent magnetic observatory observations, which are relatively few in number and poorly distributed over the Earth's surface. The severity of the problem for downward continuation of the secular variation is illustrated in figure 1. Figure 1*a*, *b* shows the radial component of the secular variation at the core surface from the 1965.0 I.G.R.F. (Zmuda 1971) and the 'definitive' model of Barraclough *et al.* (1978) for the same epoch. While many of the features are identifiable in both models, the amplitudes are consistently higher for the 'definitive' model, and the magnitude of the difference between the models is in some areas comparable with the I.G.R.F. field values themselves. Both models consist of spherical harmonic coefficients up to and including $L = 8$, and are in part based on the same data, although a considerable quantity of post-1965 data was used in the analysis by Barraclough *et al.* (1978). The most likely explanation for the lower average amplitudes for the I.G.R.F. model is that averaging the spherical harmonic coefficients of the contributory models partly averaged out the errors and reduced the amplitudes of the higher harmonics. The power spectra corresponding to figure 1*a*, *b* are plotted in figure 2, showing that the I.G.R.F. secular variation does indeed have less power in the shorter wavelength components than the 'definitive' model (a factor of 2.5 for $l = 8$).

Whaler & Gubbins (1981) describe techniques for smoothing the downward continuation process for spherical harmonic series by using estimates of the variances of the coefficients to damp the contributions from the more uncertain terms. Neither the I.G.R.F. nor the 'definitive' model have published errors, so these were estimated as the modulus of the difference between the sets of coefficients, i.e.

$$\delta \dot{g}_l^m = |(\dot{g}_l^m)_{\text{definitive}} - (\dot{g}_l^m)_{\text{I.G.R.F.}}|, \tag{2}$$

and similarly for the $\delta \dot{h}_l^m$. A smoothed 'definitive' model core secular variation field is shown in figure 1*c*. The most prominent features are the alternate 'highs' and 'lows' over the region of the core below Africa and the Indian Ocean, which can also be identified on the maps of the unsmoothed models, and the generally low values over the region beneath the Pacific. Secular variation over the Pacific at the Earth's surface is also low and has been the subject of previous investigations (e.g. Vestine & Kahle 1966). Identical smoothing of the I.G.R.F. secular variation gives a very similar map to that shown in figure 1*c*, indicating that the two data sets do give a consistent picture of core secular variation. Further smoothing highlights the contrast between the structure below Africa and the comparatively featureless opposite hemisphere. The damping therefore discriminates between well determined core surface features, which remain as the smoothing is made more severe, and those resulting from poorly determined higher harmonics, which disappear on smoothing. Whereas significant changes are introduced by

damping the secular variation as described above, the main field smoothed in an exactly similar way alters very little, because all the harmonics are reasonably well resolved.

Finally, figure 1*d* shows the radial component of the core secular variation produced by the method of Shure *et al.* (1982), using the difference between annual means for 1974 and 1959 at 106 permanent magnetic observatories. The technique of Shure *et al.* (1982) is designed to produce spatially smooth radial field components, the degree of smoothness being measured by the r.m.s. misfit between the data and the values predicted by the models at the observatory sites. Figure 1*d* has many similarities to figure 1*c*, the smoothed 'definitive' model, both in the shape and amplitudes of the features. This is remarkable considering that figure 1*d* was derived from just 318 data (three orthogonal components at the 106 stations), compared with many thousands for the 'definitive' model. In contrast, a least-squares analysis of the same data up to degree and order six produced a highly oscillatory radial secular variation component on downward continuation. This suggests that the method of Shure *et al.* (1982) may be a powerful technique for extracting information from small data sets.

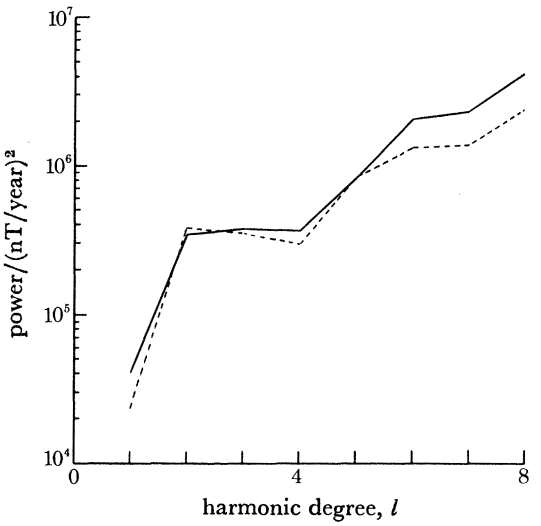

FIGURE 2. Power spectra for the 'definitive' and I.G.R.F. secular variation, plotted against harmonic number. Note that the vertical axis is logarithmic. —, 'Definitive' model; - - -, I.G.R.F.

The smooth models illustrated here show that there is information about the core field in the data, and some predominant features are emerging. The next stage, once a consistent picture has been obtained, is to examine the core motions responsible for the secular variation. Some preliminary investigations are described in the remainder of this paper, from which it will be seen how crucial good secular variation models are.

3. FLUID UPWELLING AT THE CORE SURFACE

It is now widely accepted that motions of the electrically conducting fluid of the Earth's liquid outer core are responsible for the generation of the magnetic field and its secular change. On the timescale of decades to centuries, Roberts & Scott (1965) have shown that ohmic diffusion can be neglected, i.e. that the electrical conductivity of the core is effectively infinite. If this 'frozen-flux' assumption is made, only the radial component of the magnetic field is continuous across the conductivity jump at the c.m.b. Neglecting diffusion, the radial

component of the induction equation, which relates the magnetic field and its time derivative to the fluid velocity, at the c.m.b. is

$$\dot{B}_r + \boldsymbol{v}\cdot\nabla_H B_r + B_r \nabla_H \cdot \boldsymbol{v} = 0, \tag{3}$$

where B_r is the radial field component, $\boldsymbol{v}$ the fluid velocity (which has no radial component), a dot denotes differentiation with respect to time, and $\nabla_H = \nabla - \hat{\boldsymbol{r}}(\hat{\boldsymbol{r}}\cdot\nabla)$, involving only horizontal derivatives. This equation alone, however, is not sufficient to determine the velocity field at the c.m.b. uniquely. The ambiguity is clearly pointed out by Backus (1968), who shows how to compute all velocity fields compatible with the B_r and $\dot{B}_r$ fields. Besides the velocity field itself, a description of the convective state of the core is provided by the strength and pattern of the fluid upwellings and downwellings. A quantitative measure of this is $\partial v_r/\partial r$,

TABLE 1. SECULAR CHANGE AND HORIZONTAL DIVERGENCE OF THE CORE FLOW AT CRITICAL POINTS OF $\dot{B}_r$ FOR THE I.G.R.F. 1965.0

(The first 20 points are extrema, all but one used by Whaler (1980), and the remaining 18 are saddle points yielding new data.)

no.	lat.	long.	$\dot{B}_r/(10^3$ nT/year)	$\nabla_H\cdot\boldsymbol{v}$ / 10^{-3} nT/year
1	81	−31	−0.77	−17.46
2	56	111	−0.00	−0.06
3	53	45	−0.71	5.73
4	51	−92	−0.45	−0.69
5	42	−3	−0.32	−0.99
6	38	164	0.35	7.63
7	29	−41	−1.95	12.79
8	25	59	−2.10	−4.13
9	9	−170	−0.75	2.25
10	−4	−10	−0.68	−1.66
11	−8	33	−2.34	−3.87
12	−13	84	2.85	5.53
13	−20	−93	1.18	5.04
14	−28	176	0.43	−1.13
15	−33	−9	0.01	−15.01
16	−38	48	−0.16	−0.60
17	−48	−65	1.21	4.42
18	−55	−12	0.95	5.76
19	−58	113	1.00	1.70
20	−73	−135	1.76	2.57
21	69	179	−1.42	4.81
22	64	35	0.25	−15.60
23	51	−38	3.13	−15.15
24	39	1	0.69	−2.17
25	35	81	0.56	−16.07
26	26	−38	−0.93	6.09
27	17	−142	−1.64	10.26
28	11	154	−0.46	4.41
29	−7	61	−2.15	−6.78
30	−8	4	−1.38	−3.79
31	−20	−61	0.95	9.23
32	−28	162	−1.66	−4.42
33	−31	91	−0.43	−1.03
34	−33	−102	−0.20	−0.97
35	−38	−29	−0.34	−5.25
36	−39	9	4.25	78.46
37	−68	−20	0.09	0.74
38	−71	136	−0.84	−1.51

which equals $-\nabla_H \cdot \boldsymbol{v}$ by the assumption of incompressibility, used to write (3) in the form in which it appears here. From (3), point estimates of $\nabla_H \cdot \boldsymbol{v}$ can be made where $\nabla_H B_r$ vanishes, i.e. at local extrema and saddle points of B_r, and spatial averages evaluated by integrating $\dot{B}_r$ over areas of the c.m.b. bounded by contours of B_r (Whaler 1980). In particular, if there is no upwelling at the core surface, as in a recently published thermal history calculation for the core

TABLE 2. MEANS AND STANDARD DEVIATIONS OF SECULAR CHANGE VALUES AT SETS OF POINTS FOR THE I.G.R.F. 1965.0

(The first line is for the 38 critical points. The subsequent lines are for randomly generated sets of 38 points on the c.m.b., arranged in order of increasing standard deviation. An asterisk indicates that the mean is inconsistent with zero at the 95% level.)

	mean / 10^3 nT/year	standard deviation / 10^3 nT/year	
	0.02	1.45	critical points
	−0.08	1.57	
	0.18	1.68	
	−0.08	1.72	
	0.07	1.74	
	0.55*	1.74	
	−0.18	1.78	
	−0.05	1.82	
	−0.004	1.83	
	0.29	1.84	
	0.11	1.90	
	0.08	1.96	
	0.20	1.97	
	0.42	1.99	
	−0.06	2.00	
	−0.14	2.00	
	−0.13	2.05	
	−0.07	2.05	
	0.18	2.06	
	0.12	2.10	
	−0.10	2.13	
	0.10	2.16	
	−0.20	2.17	
	−0.76	2.26	
	−0.21	2.43	
overall	0.04	1.95	

(Gubbins *et al.* 1982), $\dot{B}_r$ must vanish at the critical points (local extrema and saddle points) of B_r. The close proximity of zero $\dot{B}_r$ contours to the extrema led Whaler (1980) to explore the possibility that the I.G.R.F. is compatible with no upwelling. Since there are no error estimates on either the $\dot{B}_r$ field or the positions of the critical points, the question was addressed statistically: compared with random $\dot{B}_r$ values on the core surface, do those at the extrema deviate less from zero? An F test to compare the variances of the extremal and randomly generated $\dot{B}_r$ values gave a result statistically significant at the 5% level (Whaler 1980). Including saddle point data (and an additional extremum) strengthens the result. The values of $\dot{B}_r$ and $\nabla_H \cdot \boldsymbol{v}$ at the 38 critical points (20 extrema and 18 saddle points) are shown in table 1. In some cases the value of $\nabla_H \cdot \boldsymbol{v}$ is quite large even though the angular distance between the critical point and the nearest zero contour of $\dot{B}_r$ is small. This happens when spatial gradients of $\dot{B}_r$ in the vicinity of the critical point are large, or if the value for B_r at the critical point is small. The mean and standard deviation of the $\dot{B}_r$ values of table 1, together with those for

24 sets of randomly generated points, are given in table 2. The means of all but one of the randomly generated sets are consistent with zero at the 95% level, with a two-tailed Student's t test. This is to be expected since $\dot{B}_r$ averages to zero over a sphere. However, every set of randomly generated $\dot{B}_r$ values has a larger standard deviation, indicating that they are more variable about zero than the critical point values. This was quantified by a one-tailed F test on the null hypothesis that the variances of the randomly generated and critical point $\dot{B}_r$ values are equal, tested against that of the random values being larger. The overall standard deviation of the random values, obtained by combining the 24 sets of table 2, is 1.95; the null hypothesis can be rejected at the 99% level. Thus the additional data are consistent with the hypothesis that $\nabla_H \cdot \boldsymbol{v} = 0$.

Further support for this hypothesis comes from an r.m.s. error estimate for $\dot{B}_r$, using a formula of Lowes (1966) and the $\delta\dot{g}_l^m$ and $\delta\dot{h}_l^m$ of (2). This gives $\delta\dot{B}_r = 1.73 \times 10^3$ nT per year. From table 1, 30 of the critical points have a $\dot{B}_r$ value within this bound. If $\delta\dot{B}_r$ were the one standard deviation value, two-thirds of the $|\dot{B}_r|$ values of a normal sample should be less than this; that the bound encompasses a much higher fraction is again indicative of below average $\dot{B}_r$ values at the critical points.

The test described above was also applied to the 'definitive' model. The $\dot{B}_r$ values at the 40 critical points had a standard deviation of 2.07×10^3 nT per year, which exceeded that of 2 out of 24 random sets. However, the overall standard deviation of the randomly generated values was 2.43×10^3 nT per year, and the null hypothesis of equal variances could be rejected at the 95% level, lower than for the I.G.R.F., but still statistically significant.

The test was then repeated for several smoother secular variation models (produced by applying Whaler & Gubbins's (1981) methods to existing spherical harmonic models or by the Shure *et al.* (1982) method), including those in figure 1*c*, *d*. A correlation between the smoothness of the model and the rejection level of the null hypothesis emerged, with a lower rejection level for smoother models. In all cases, the variance of the critical point $\dot{B}_r$ values was less than that for random points, but the result of an F test was not statistically significant, i.e. the rejection level was below 95% for models similar to, or smoother than, those shown in figure 1*c*, *d*.

On the basis of critical point data, both the I.G.R.F. and 'definitive' models are compatible with no upwelling at the c.m.b. The evidence from smoother secular variation models is less convincing, although it does not contradict the hypothesis. Therefore, in the absence of strong evidence to the contrary, the assumption of zero upwelling is a useful first approximation. The velocity ambiguity in (3) is then reduced, for the component perpendicular to contours of B_r can be calculated everywhere on the c.m.b.

4. Is horizontal motion dominated by azimuthal flow?

The results of the previous section suggest that upwelling of the core fluid at the c.m.b., if it exists, cannot be detected with currently available field models. This could be due to the poor signal:noise ratio in the fields after extrapolation to the c.m.b., and the question then arises whether *any* fluid motions can be resolved above the noise level. In this section, therefore, the east–west and north–south components of horizontal fluid flow on null-flux curves at the c.m.b., which are uniquely determined by the induction equation, are evaluated and compared for the I.G.R.F. and 'definitive' field models. The results will also be examined in an attempt

to determine whether the westward drift of the geomagnetic field (Bullard *et al.* 1950) is associated with azimuthal fluid flow.

The east–west components of flow on null-flux curves are uniquely determined where the null-flux curves run locally north–south; similarly the north–south flow can be calculated where null-flux curves are east–west orientated. Besides the magnetic equator, there are four closed null-flux curves for both models, two each in the Northern and Southern Hemispheres.

TABLE 3. NORTH–SOUTH AND EAST–WEST VELOCITY COMPONENTS ON NULL-FLUX CURVES FOR THE I.G.R.F. AND 'DEFINITIVE' SECULAR VARIATION MODELS, AND AFTER SMOOTHING

(The velocities are in kilometres per year, positive north and east. For the north–south velocity components, the most northerly point of the closed loops appears first. Points on the magnetic equator are arranged in order of increasing longitude. For the east–west components, the most westerly point appears first. The final value in each column is the r.m.s. value of $\dot{B}_r$.)

	velocity/(km/year)			
location	I.G.R.F.	definitive	I.G.R.F., smoothed	definitive, smoothed
	north–south components			
N Pacific	−2.69	−9.56	−5.68	−5.58
	−6.65	−12.21	−7.82	−5.32
S Africa	−3.12	−5.37	−1.7	−3.47
	13.31	17.04	12.99	14.38
S America	1.88	−4.56	1.25	−1.83
	1.68	1.00	2.93	1.21
magnetic equator	0.95	−1.88	0.66	−0.97
	1.05	1.9	1.10	0.5
	−5.63	−5.89	−4.08	−3.24
	0.31	3.59	−1.37	0.04
	−4.1	−9.19	−6.16	−9.15
	−4.42	−3.29	−2.67	0.35
	3.98	3.15	2.67	0.38
	12.71	−1.51	8.94	1.69
	26.47	12.48	18.48	12.85
	−3.18	10.54	1.41	10.09
	3.96	19.41	2.08	11.15
	−4.01	−0.35	−2.89	−0.17
	east–west components			
N Pacific	8.49	13.84	6.25	6.35
	−39.07	−11.67	−29.58	−13.10
S Africa	−18.92	−17.43	−17.8	−12.29
	−6.99	−15.46	−5.23	−8.41
S America	−4.58	−0.65	−2.94	−3.21
	−4.41	−6.13	−3.96	−5.90
$\langle\dot{B}_r\rangle$/(10^3 nT/year)	1.96	2.40	1.55	1.73

Their positions and sizes vary slightly between the two models, but lie approximately over areas beneath the North Pole, the North Pacific, South Africa and South America. This gives potentially eight points where the null-flux curves run locally east–west or north–south; however, those associated with the most northerly null-flux curve will not be considered because directions are not well determined so close to the North Pole. In addition, the magnetic equator gives another twelve points where the north–south velocity component can be uniquely determined, but no east–west components. These velocity components are displayed for the I.G.R.F. and 'definitive' models in the first two columns of table 3. The magnitudes are typically lower for the I.G.R.F. because the velocity component is directly proportional to $\dot{B}_r$

(equation (3) with $B_r = 0$), which tends to be smaller for the I.G.R.F. (compare figure 1*a* with figure 1*b*). The velocities in the fourth column correspond to the smoothed 'definitive' secular variation of figure 1*c*, and in the third column to the I.G.R.F. smoothed in the same way; velocities obtained from these smoothed $\dot{B}_r$ fields have in general lower magnitudes for the same reason. For a purely azimuthal flow, (3) shows that $\dot{B}_r$ must vanish wherever the null-flux curves run locally east–west; these $\dot{B}_r$ values are displayed for the 'definitive' model in table 4, which does not suggest that this is so. The same conclusion can be drawn from a map of the null-flux curves at the c.m.b. with zero $\dot{B}_r$ contours superimposed, shown for the 'definitive' model in figure 3. Some points where the north–south velocity component can be determined are close to a zero $\dot{B}_r$ contour, but at others, the angular distance to a zero $\dot{B}_r$

TABLE 4. SECULAR CHANGE VALUES AT POINTS WHERE THE NORTH–SOUTH VELOCITY COMPONENT CAN BE CALCULATED FOR THE 'DEFINITIVE' SECULAR VARIATION

location	$\dot{B}_r/(10^3$ nT/year)	location	$\dot{B}_r/(10^3$ nT/year)
N Pacific	2.03	magnetic equator	1.07
	−1.63		−1.45
S Africa	−2.58		3.70
	−3.77		−1.34
S America	−1.25		2.59
	−0.42		0.76
			−1.54
			0.43
			−2.28
			−1.95
			−4.93
			0.15

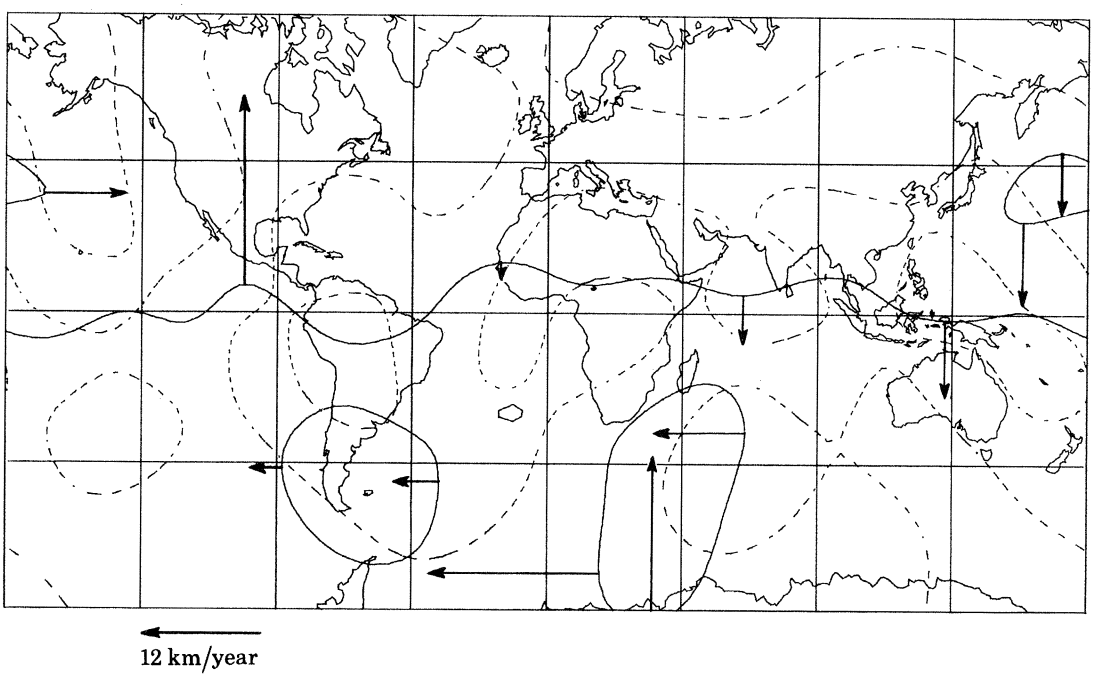

FIGURE 3. Null-flux curves (solid contours) for the 'definitive' model and zero radial secular variation contours (broken contours). Well determined north–south and east–west velocity components are also plotted. 12 km/year ≈ 0.2°/year, the westward drift speed of the geomagnetic field.

contour reaches almost its maximum value. Furthermore, by using an F test in the same way as at critical points, the evidence to suggest that the radial secular variation values at these points is less than elsewhere is weak (the null hypothesis of equal variances cannot be rejected at any statistically significant level). In fact, the random points do have a larger variance, but several points on the east–west null-flux curves have $\dot{B}_r$ values above average.

Looking across the columns of table 3, there is no correlation between the velocity components predicted by the various secular variation models at some points, but at others there seems to be a reasonable correspondence in sign and magnitude, bearing in mind the variation in amplitude of the $\dot{B}_r$ field between models. This variation is reflected in the r.m.s. value of $\dot{B}_r$ over the sphere for each model, calculated by using Lowes's (1966) formula and displayed at the foot of each column of table 3. The result of picking out the velocity components that seem to show some consistency between models, normalizing by the ratio of the r.m.s. $\dot{B}_r$ values (relative to the I.G.R.F.) and averaging is plotted in figure 3. The east–west flow is mainly westward, at typically half the westward drift speed of the geomagnetic field. However, there is significant north–south flow at some points on the c.m.b., and, statistically, no difference in magnitude between the east–west and north–south flows can be found. Gubbins (this symposium) has used the assumption of no fluid upwelling to calculate velocity components perpendicular to contours of B_r over the whole c.m.b. The flow pattern in the vicinity of null-flux curves is consistent with that shown in figure 4.

In conclusion, it can be seen that there is information in the secular variation data about the fluid motions at the core surface. Significant flow in both the east–west and north–south directions has been resolved, and there is no evidence to suggest that the westward drift of the geomagnetic field is associated with azimuthal flow (see also Gubbins 1982), although the well resolved longitudinal flow tends to be westward.

5. Conclusions

The problem of instability in the downward continuation of spherical harmonic models has been examined for the geomagnetic secular variation, and methods for producing spatially smoother estimates have been illustrated. It is difficult to determine the appropriate level of damping, but it may be possible to base a decision on an integral constraint arising from the frozen-flux assumption. The induction equation was used to infer some general properties of the fluid flow at the c.m.b. Firstly, the absence of fluid upwelling is an assumption compatible with the data. This reduces the velocity ambiguity inherent in the induction equation. Secondly, there are points at which the meridonal component of velocity is significant. There are only six points at which the azimuthal velocity component can be estimated, and at all but one the flow is westward, at typically half the westward drift speed of the geomagnetic field. However, it must be borne in mind that the reliability of the velocity information deduced from the induction equation depends strongly on the reliability of the c.m.b. secular variation. Until there is a wider consensus of agreement between models, or we can place error bounds on individual values, the results of such studies must be treated with some caution.

Thanks are due to Loren Shure for the use of field models based on her method prior to publication, and to David Gubbins and Edward R. Benton for suggestions about the meridonal velocity. Financial support for this work came from the N.E.R.C., partly under grant no. GR3/3475.

PHILOSOPHICAL TRANSACTIONS OF THE ROYAL SOCIETY A MATHEMATICAL, PHYSICAL & ENGINEERING SCIENCES

References (Whaler)

Backus, G. E. 1968 *Phil. Trans. R. Soc. Lond.* A **263**, 239–266.
Barraclough, D. R. & Malin, S. R. C. 1971 *Inst. geol. Sci. rep.* no. 71/1. (26 pages.)
Barraclough, D. R., Harwood, J. M., Leaton, B. R. & Malin, S. R. C. 1978 *Geophys. Jl R. astr. Soc.* **55**, 111–121.
Benton, E. R. 1979*a* *Geophys. Astrophys. fluid Dynam.* **11**, 323–327.
Benton, E. R. 1979*b* *Phys. Earth planet. Inter.* **20**, 111–118.
Benton, E. R. 1981 *Phys. Earth planet. Inter.* **24**, 242–244.
Benton, E. R. & Muth, L. A. 1979 *Phys. Earth planet. Inter.* **20**, 127–133.
Booker, J. R. 1969 *Proc. R. Soc. Lond.* A **309**, 27–40.
Bullard, E. C., Freedman, C., Gellman, H. & Nixon, J. 1950 *Phil. Trans. R. Soc. Lond.* A **243**, 67–92.
Gubbins, D., Thomson, C. J. & Whaler, K. A. 1982 *Geophys. Jl R. astr. Soc.* **68**, 241–251.
Lowes, F. J. 1966 *J. geophys. Res.* **71**, 2179.
Roberts, P. H. & Scott, S. 1965 *J. Geomagn. Geoelect., Kyoto* **17**, 137–151.
Shure, L., Parker, R. L. & Backus, G. E. 1982 *Phys. Earth planet. Inter.* (In the press.)
Vestine, E. H. 1952 *Proc. natn. Acad. Sci. U.S.A.* **38**, 1030–1038.
Vestine, E. H. & Kahle, A. B. 1966 *J. geophys. Res.* **71**, 527–530.
Whaler, K. A. 1980 *Nature, Lond.* **287**, 528–530.
Whaler, K. A. & Gubbins, D. 1981 *Geophys. Jl R. astr. Soc.* **65**, 645–693.
Zmuda, A. J. 1971 *IAGA Bull.* no. 28.

Discussion

F. J. Lowes (*School of Physics, University of Newcastle upon Tyne, U.K.*). To reduce the effect of high harmonics on the core surface field Dr Whaler has used a smooth weighting function (filter) in the (spatial) frequency (spherical harmonic) domain. Such smooth functions are normally used in the space (or time) domain to avoid the secondary response lobes in the frequency domain, but as Dr Whaler is already working in the frequency domain it would be easier and more logical simply to truncate.

Kathryn A. Whaler. The point is that here we have frequency 'data', whereas we are interested in estimates of the spatial function, the reverse of the normal situation. Thus the whole process is inverted, and a smooth filter is applied in the frequency domain, which reduces the amplitudes of the secondary lobes of the response in the spatial domain compared with straightforward truncation. Whaler & Gubbins (1981) discuss and illustrate this in more detail.

PHILOSOPHICAL TRANSACTIONS OF THE ROYAL SOCIETY A MATHEMATICAL, PHYSICAL & ENGINEERING SCIENCES